

Center-to-limb variations in coronal hole and quiet Sun regions obtained with IRIS spectroscopic observations

Pradeep Kayshap,¹* Peter R. Young^{2,3}

¹ School of Advanced Sciences and Languages, VIT Bhopal University, Kothrikalan, Sehore Madhya Pradesh - 466114

² NASA Goddard Space Flight Center, Greenbelt, MD, USA

³ Department of Mathematics, Physics and Electrical Engineering, Northumbria University, Newcastle upon Tyne, UK

Accepted XXX. Received YYY; in original form ZZZ

ABSTRACT

The center-to-limb variations (CLV) of Gaussian fit parameters of the transition region Si iv 1402.77 Å spectral line in quiet Sun (QS) and coronal hole (CH) regions are presented. The results are derived from a full-disk mosaic scan obtained by the Interface Region Imaging Spectrograph on 24 September 2017. The CLV for a CH transition region line has not previously been reported, and the parameters are found to show variations consistent with the QS. The intensity increases towards the limb, consistent with an increasing plasma column depth due to line-of-sight effects. The Doppler velocity is normalized to be zero at the limb for both QS and CH and increases to +4.8 km s⁻¹ (redshift) at disk center for CH and +5.2 km s⁻¹ for QS. Non-thermal broadening in the CH decreases from a maximum of 24 km s⁻¹ at the limb to 10 km s⁻¹ at disk center. For QS the broadening decreases from 25 km s⁻¹ at the limb to 14 km s⁻¹ at disk center. Both Doppler velocities and non-thermal velocities vary linearly with cos θ, where θ is the heliocentric angle. The QS results for both parameters are consistent with earlier work.

Key words: Sun: transition region – Sun: atmosphere – Sun: UV radiation

1 INTRODUCTION

Ultraviolet emission lines formed in the solar transition region (TR) at temperatures of 10⁵ K have long been known to exhibit Doppler redshifts and broadening in excess of the thermal broadening. [Doschek et al. \(1976\)](#) were the first to report redshifts in TR lines from a study of *Skylab* S082-B spectra, finding Doppler shifts of up to 15 km s⁻¹. Enhanced non-thermal broadening at TR temperatures around 10⁵ K was first reported by [Boland et al. \(1973\)](#). Both results likely give clues on the how mass and energy are balanced in the solar atmosphere. For example, non-thermal broadening may be caused by the passage of magnetohydrodynamic waves through the TR, while ubiquitous downflows in the TR represent mass and energy loss terms that need to be balanced to maintain a hot corona (see [Mariska 1992](#), for more details).

One method for characterizing the TR non-thermal broadening and Doppler shifts is to measure the emission line properties at different positions on the Sun, from the center of the disk to the limb. Variations in the parameters then give clues as to the origin of the two effects. For example, if plasma flows are along radially-aligned structures then net Doppler shifts would be expected to be at a maximum at disk center and fall to zero at the limb. Similarly, if non-thermal broadening is due to random, lateral motions of radially-aligned structures then it would be expected to be largest at the limb and fall to zero at disk center (the motions giving a distribution of Doppler shifts when the line-of-sight is aligned to the motions).

In the present work we present the center-to-limb variation (CLV) of the Doppler velocity and non-thermal broadening of the Si iv

1402.77 Å TR emission line in both quiet Sun and coronal hole conditions across the full range of heliocentric angles. Although such a study has been performed for the quiet Sun previously, the present work is the first for coronal holes. Si iv is formed at around 80 kK in the solar atmosphere, and the earlier work of [Peter & Judge \(1999\)](#) suggests this line should show a redshift of 5–8 km s⁻¹ at disk center in the quiet Sun.

CLV of emission line properties has been studied in various ways with spectrometers in the past. The HRTS rocket experiment had a long slit that could be positioned to extend from disk center to the limb. [Dere et al. \(1984\)](#) studied the CLV of several lines, including the C iv 1548 Å 1550 Å doublet, and [Brekke \(1993\)](#) looked at the CLV of two O v lines. Another rocket experiment performed an east-west scan across the equator, with results for several lines presented in [Rottman et al. \(1990\)](#) and [Hassler et al. \(1991\)](#). Spacecraft enable long-duration observations and full-disk raster scans were performed with the Solar Ultraviolet Measurements of Emitted Radiation (SUMER: [Wilhelm et al. 1995](#)). These have been used to study the CLV of several lines ([Peter 1999](#)). These studies all yield continuous data from disk center to the limb, either with a single observation or with a patchwork of multiple spacecraft pointings. As spacecraft spectrometers usually have a restricted field-of-view, authors sometimes combine observations obtained at different times and pointings to investigate CLV ([Doschek et al. 1976](#); [Rao et al. 2022](#)). In the present work we use IRIS data obtained with a full disk scan, analogous to the study of [Peter \(1999\)](#).

For studying the Doppler shift CLV, an important consideration is the reference wavelength used to derive the line-of-sight velocity. Within a single spectrum a common procedure is to assume a chromospheric emission line within the spectrum has a zero Doppler

* E-mail: virat.com@gmail.com

velocity, which then fixes the absolute calibration of that spectrum. The measured wavelength of the TR line is then compared with the known rest wavelength to yield the Doppler velocity. Tables of rest wavelengths are given in Brekke et al. (1997) and Kelly (1987). The TR Doppler velocities would be expected to go to zero at the limb, and this was validated by Rottman et al. (1990) and Peter & Judge (1999). The earlier work of Dere et al. (1984) suggested this may not be the case, but Brekke et al. (1997) argued that a single slit position (such as used for the Dere et al. 1984, observation) may lead to non-zero Doppler shifts at the limb, but a spatial average (multiple slit positions) will lead to an average zero Doppler velocity.

Peter & Judge (1999) provided quiet Sun Doppler velocity CLV data for 10 ion species, fitting the results with a $\cos \theta$ function (θ the heliocentric angle). Only the spatial region $750''$ to $1000''$ was fit and so the disk center velocity was inferred from the $\cos \theta$ form of the fit. The results were obtained from a special observation where the SOHO spacecraft was progressively rolled through 30° steps with the SUMER slit positioned $70''$ inside the limb. Some coronal hole data were available from this dataset, and Peter & Judge (1999) provided CLV curves for eight ion species. The spatial region that could be fit was smaller than for the quiet Sun, and varied with ion species. The authors noted that the ion C IV, formed at a similar temperature to the Si IV considered in the present work, showed a CLV behavior significantly different to the quiet Sun. Inspection of the authors' Figure 5 shows Doppler velocities that are slightly positive compared to -1 to -2 km s^{-1} in the quiet Sun.

TR emission line widths have generally been found to be approximately constant from disk center to the limb, with a small increase at the limb (Feldman et al. 1976; Chae et al. 1998). The limb increase found by Doyle et al. (2000) for C IV was interpreted as due to opacity effects at the limb. Erdelyi et al. (1998) found larger enhancements in the limb non-thermal broadening, with enhancement values up 8 km s^{-1} for lines formed close to the temperature of Si IV. This result was interpreted as evidence of Alfvén waves passing through the TR. Most recently, Rao et al. (2022) studied the CLV of the non-thermal broadening of Si IV using IRIS data, finding a limb non-thermal velocity of 20 km s^{-1} and a disk center velocity of 15 km s^{-1} , supporting the earlier Erdelyi et al. (1998) result.

Section 2 presents the observational dataset used in the present work. Section 3 describes the analysis method and gives the center-to-limb variation for the Si IV emission line parameters. Finally, the results are summarized in Section 4.

2 OBSERVATION AND DATA ANALYSIS

The Interface Region Imaging Spectrometer (IRIS: De Pontieu et al. 2014) provides high-resolution imaging and spectroscopic data at near ultraviolet (NUV) and far ultraviolet (FUV) wavelengths. In the FUV spectrum are two strong lines at 1393.77 \AA and 1402.77 \AA that are due to Si IV, an ion formed in the TR at a temperature around 80 kK . The 1402.77 \AA line is the subject of the present study.

IRIS has a slit of length $175''$ and width $0.33''$, and spectroscopic images are built up through rastering. For the full-disk mosaic observations, 64-step rasters are used, and the step size is $2''$. Multiple, consecutive spacecraft pointings are required to observe the full solar disk. The mosaics are performed regularly as part of the IRIS synoptic program (Gunár et al. 2021). These data are ideal for studying CLV of emission line properties.

In the present work we use the full-disk mosaic obtained between 13:09 UT on 24 September 2017 and 06:33 UT on 25 September. The mosaic comprised 185 coarse raster scans, each with an exposure

time of 2 s. The IRIS team assembles the individual rasters into a single 3D data cube (x, y, λ) for each emission line, and makes them available at the [IRIS Full Disk Mosaic website](#).

In order to study the CLV within a coronal hole, it is necessary to clearly identify the coronal hole boundary within the IRIS full-disk mosaic image. For this purpose we used co-temporal 193 \AA images from the Atmospheric Imaging Assembly (AIA: Lemen et al. 2012) on the Solar Dynamics Observatory (SDO: Pesnell et al. 2012). This channel is dominated by Fe XII lines formed at around 1.5 MK that clearly reveal the coronal hole locations. By matching the observation times and spatial locations of IRIS, AIA 193 \AA images were assembled into a mosaic that shows the co-temporal coronal conditions for the IRIS mosaic. The left panel of Figure 1 shows the AIA 193 \AA mosaic, and the right panel shows the IRIS Si IV mosaic. The coronal hole contours derived from the 193 \AA image are over-plotted on both full-disk images.

The Si IV 1402.77 \AA full-Sun mosaic datacube was downloaded for the present study, and gives the spectral radiances for each spatial pixel of the solar disk. Uncertainties on the spectral radiances were derived using the procedure contained in the SSW IDL routine `iris_getwindata.pro`. The Si IV 1402.77 \AA image shown in Figure 1 was generated by first binning the mosaic by two and five pixels in the x and y directions, respectively. A single Gaussian function was then fit to the line at each spatial pixel using the IDL routine `gaussfit.pro`, and the image shows the radiances from the Gaussian fit functions.

3 RESULTS

In this section we obtain distributions of the intensity, Doppler velocity, and non-thermal line width of Si IV 1402.77 \AA as a function of $\mu = \cos \theta$ for quiet Sun and coronal hole regions. θ is the heliocentric angle ($\theta = 0$ is disk center). The AIA and IRIS data used in this work provide spatial information in heliocentric coordinates. These were converted to μ values by using a solar radius of $957.3''$, obtained from the IDL routine `get_rbp` using the date 2017 September 24. The method for obtaining a reference wavelength for Si IV 1402.77 \AA , which is needed to obtain Doppler velocities, is described in Section 3.1. The selections of the QS and CH regions are discussed in Sections 3.2, and the results are presented in Sections 3.4 and 3.5.

3.1 Estimation of Rest Wavelength

To derive the Doppler velocity CLV for Si IV 1402.77 \AA it is necessary to have an absolute wavelength calibration reference. For the full-disk mosaic data used here, we assume that the 1402.77 \AA line has zero Doppler velocity at the limb ($\mu = 0$). This is implemented by defining quiet Sun and coronal hole regions (Sects. 3.4 and 3.5) within the mosaics and plotting the centroids as a function of μ . A straight line fit ($a + b\mu$) to the centroids is performed, and the parameter a is set to the reference wavelength of the line (1402.770 \AA). Further details are given in Appendix A. Therefore when the Doppler velocity is derived using the reference wavelength, the velocity at the limb is 0 km s^{-1} .

The wavelength scale of IRIS is known to drift during an orbit (IRIS Technical Note 20), which potentially affects the mosaic Doppler velocity results. However, this effect is corrected in the IRIS level-2 data used here, hence the reference wavelength is assumed the same across the mosaic.

3.2 Selection of the QS and CHs

3.2.1 Selection of the QS

The south-west quadrant of the AIA 193 Å image (Figure 1) is mostly free of CH and AR emission, and a diagonal band running from disk center to the limb was selected to derive the QS CLV. The IRIS Si iv mosaic image was first binned by 5 pixels in the y -direction. For each of 339 x -pixels along the diagonal, 109 y -pixels centered on the diagonal were extracted resulting in an array of 339 x 109 spectra. This array is overplotted on Figure 2 in blue. The μ value was derived for each pixel within this array. The Si iv line was fit to each spectrum, giving intensity, centroid, and line width data as a function of μ .

3.2.2 Selection of the CHs

The white contours on Figure 2 show the locations of two coronal holes as obtained from the Heliophysics Event Knowledgebase (HEK: Hurlburt et al. 2012). The HEK contains coronal positions generated from the Spatial Possibilistic Clustering Algorithm (SPoCA: Verbeecq et al. 2014) method. The SPoCA results within the HEK have a 6 hour cadence, and for each segment of the AIA and IRIS mosaic images, the nearest-in-time SPoCA contours were used. The IRIS mosaic image was binned by 5 pixels in the y -direction to improve signal-to-noise. Each spatial pixel of the IRIS mosaic that lies within the white contours of Figure 2 was extracted and a Gaussian fit performed to the Si iv line. The μ value for each pixel was also computed, giving the intensity, centroid and line width as a function of μ . Combined, the two coronal holes give almost complete coverage of μ from 0 to 1.

3.3 Gaussian fitting

For each pixel of the QS and CH areas described in the previous section, a Gaussian function was fit to Si iv 1402.77 Å using the IDL gaussfit function. Following Rao et al. (2022) we have rejected fits with a reduced- χ^2 value greater than five. Such fits can arise from data artifacts such as cosmic ray hits, and from non-Gaussian line profiles due to dynamic solar events, for example. The integrated line intensity is computed from the fit parameters, and the Doppler velocity is computed from the line centroid using the limb reference wavelength described in Section 3.1. The Gaussian width parameter is converted to full-width at half-maximum (FWHM), and then input to the routine eis_width2velocity, available in the SolarSoft distribution. This routine subtracts the thermal and instrumental widths and outputs the non-thermal velocity (see, e.g., Eq. 1 of Rao et al. 2022). The instrumental width is 26 mÅ (De Pontieu et al. 2014), and a temperature of $\log T = 4.87$ is used to compute the thermal width. The latter is the temperature of peak ionization of Si iv. The width of the line's emissivity function is 0.19 dex, measured as the width at half-maximum of the function.

3.4 Center-to-Limb Variations in QS

Figure 2 shows 2D histograms of the intensity, Doppler velocity and non-thermal velocity as a function of μ as derived from the Gaussian fits to the QS pixels. In order to better display the center-to-limb trends, in Figure 3 we divide the μ range into 100 equally-spaced bins and plot the mean intensity, Doppler velocity and non-thermal velocity derived from the QS pixels within each bin. The error bars show the standard deviation of the values within that bin.

Table 1. Linear fit parameters (a , b) and Pearson correlation coefficients (PCC) for the Doppler velocity, v_D , and non-thermal velocity, ξ , in the QS and CH regions. Please note that the error in each line fit parameter is the $1-\sigma$ error.

Parameter	Region	a	b	PCC
v_D	QS	0 ± 0.33	5.74 ± 0.57	0.71
	CH	0 ± 0.32	4.84 ± 0.54	0.68
ξ	QS	23.8 ± 0.65	-9.42 ± 1.12	-0.64
	CH	24.4 ± 0.41	-14.8 ± 0.69	-0.91

The Si iv intensity shows a small increase from disk center ($\mu = 1$) to $\mu = 0.2$, with a larger increase towards the limb. This is consistent with an increase in the line-of-sight column depth of the emitting plasma towards the limb.

The Doppler velocity shows a clear trend of increasing redshift towards disk center (Figure 3) and a linear fit yields the parameters shown in Table 1. The Doppler shift at disk center is 5.2 km s^{-1} . Peter & Judge (1999) presented the CLV for Si iv 1402.77 Å for a reduced range of μ values, and the fit to their data is overplotted in blue on the second panel of Figure 3. The fit implies a redshift at disk center of $4.8 \pm 1.1 \text{ km s}^{-1}$, in excellent agreement with the value found here.

The non-thermal velocity shows a clear decrease from the limb to disk center, and a linear fit yields the parameters shown in Table 1. The non-thermal velocity at the limb is 25 km s^{-1} and at disk center is 14 km s^{-1} . Rao et al. (2022) found values of around 20 km s^{-1} at the limb, and around $14\text{--}17 \text{ km s}^{-1}$ near disk center using the Si iv 1393.75 Å line.

3.5 Center-to-Limb Variations in CHs

Figures 4 and 5 are directly analogous to Figures 2 and 3, but for the CH data. Although there is almost complete coverage of the μ angles, there are relatively few pixels below $\mu = 0.1$ and in the range $0.55 \leq \mu \leq 0.75$. The behaviors of the intensity, Doppler velocity and nonthermal velocity are consistent with the QS dataset. The intensity shows a small increase to about $\mu = 0.2$, and a larger increase towards the limb.

The Doppler velocity shows a clear linear relationship with μ (Figure 5, middle panel), and the linear fit parameters are given in Table 1. The velocity at disk center is 4.8 km s^{-1} , very similar to the value found in the QS. Peter & Judge (1999) did not provide Doppler velocity measurements in the coronal hole from Si iv, but they did give values for C iv, which is a slightly hotter ion ($\log T = 5.05$). The fit from this work is over-plotted on the middle panel of Figure 5 as a blue line, and it can be seen that the line is actually blue-shifted. Our work contradicts this measurement.

The non-thermal velocity also shows a clear linear relationship with μ (Figure 5, lower panel), and the linear fit parameters and Pearson correlation coefficient are given in Table 1. The velocity at the limb is very similar to that found for the QS, but the disk center value is lower, at 9.6 km s^{-1} .

4 DISCUSSION AND CONCLUSIONS

We have presented the first-ever measurement of the center-to-limb variation of Gaussian line-fit parameters for a solar transition region line (Si iv 1402.77 Å) in a coronal hole. We have used data from an IRIS full-disk mosaic dataset that includes a coronal hole that

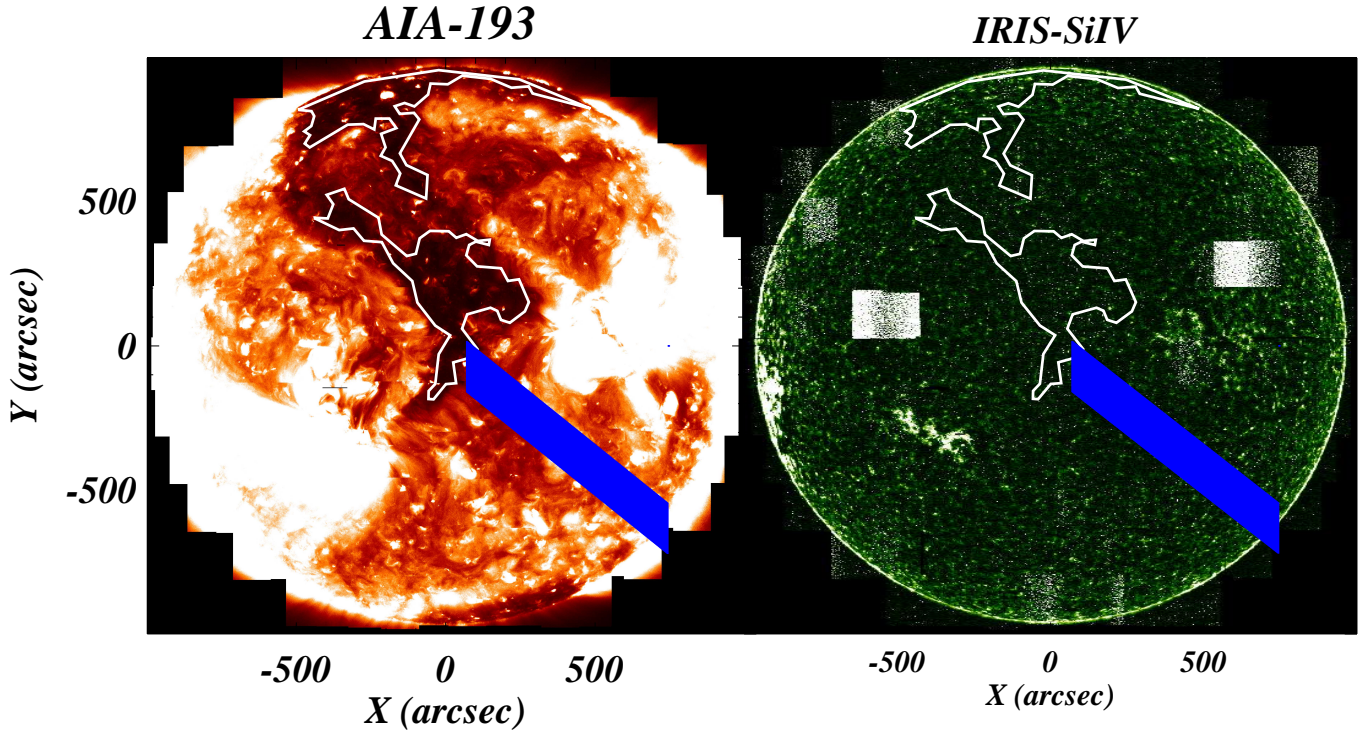


Figure 1. The right panel shows the IRIS full-disk mosaic image from the Si iv 1402.77 Å line. The left panel shows a mosaic image constructed from AIA 193 Å images that were chosen to match the timing and pointing data from the IRIS mosaic. The QS region used for the CLV study is shown by a slanted blue patch that extends from the disk center towards the southwest limb of the Sun. White contours denote the two CHs that were used for the CLV study.

extends to disk center. The line intensity increases towards the limb, consistent with an increasing plasma column depth due to line-of-sight effects. The Doppler velocity and non-thermal velocity show linear variations with μ . The former is normalized to zero velocity at the limb, and displays an increasing redshift towards disk center. The disk center velocity is 4.8 km s^{-1} . The non-thermal velocity decreases from 24 km s^{-1} at the limb to 10 km s^{-1} at disk center.

The same procedures were applied to a section of quiet Sun, and similar results were found. The redshift at disk center is 5.2 km s^{-1} , and the non-thermal velocity decreases from 25 km s^{-1} at the limb to 14 km s^{-1} at disk center.

The quiet Sun Doppler velocity results are consistent with those from Peter & Judge (1999), but the coronal hole results are significantly different. Peter & Judge (1999) found blue-shifted emission in a coronal hole from C iv, which is a slightly hotter ion than Si iv. Rao et al. (2022) recently measured non-thermal velocities in the quiet Sun using the IRIS Si iv 1393.75 Å line, and they found similar values at disk center but slightly lower velocities of 20 km s^{-1} at the limb.

ACKNOWLEDGEMENTS

PRY acknowledges support from the GSFC Internal Scientist Funding Model competitive work package program. IRIS is a NASA Small Explorer mission developed and operated by LMSAL with mission operations executed at NASA Ames Research Center and major contributions to downlink communications funded by ESA and the Norwegian Space Centre. We also acknowledge the data from SDO/AIA.

DATA AVAILABILITY

We used spectroscopic data from IRIS and imaging observations (i.e., AIA 193 Å mosaic) from AIA/SDO instruments, and the complete set of data is available at https://www.lmsal.com/solarsoft/irisa/data/level2_compressed/2

REFERENCES

- Boland B. C., Engstrom S. F. T., Jones B. B., Wilson R., 1973, *A&A*, **22**, 161
- Brekke P., 1993, *ApJ*, **408**, 735
- Brekke P., Hassler D. M., Wilhelm K., 1997, *Sol. Phys.*, **175**, 349
- Chae J., Schühle U., Lemaire P., 1998, *ApJ*, **505**, 957

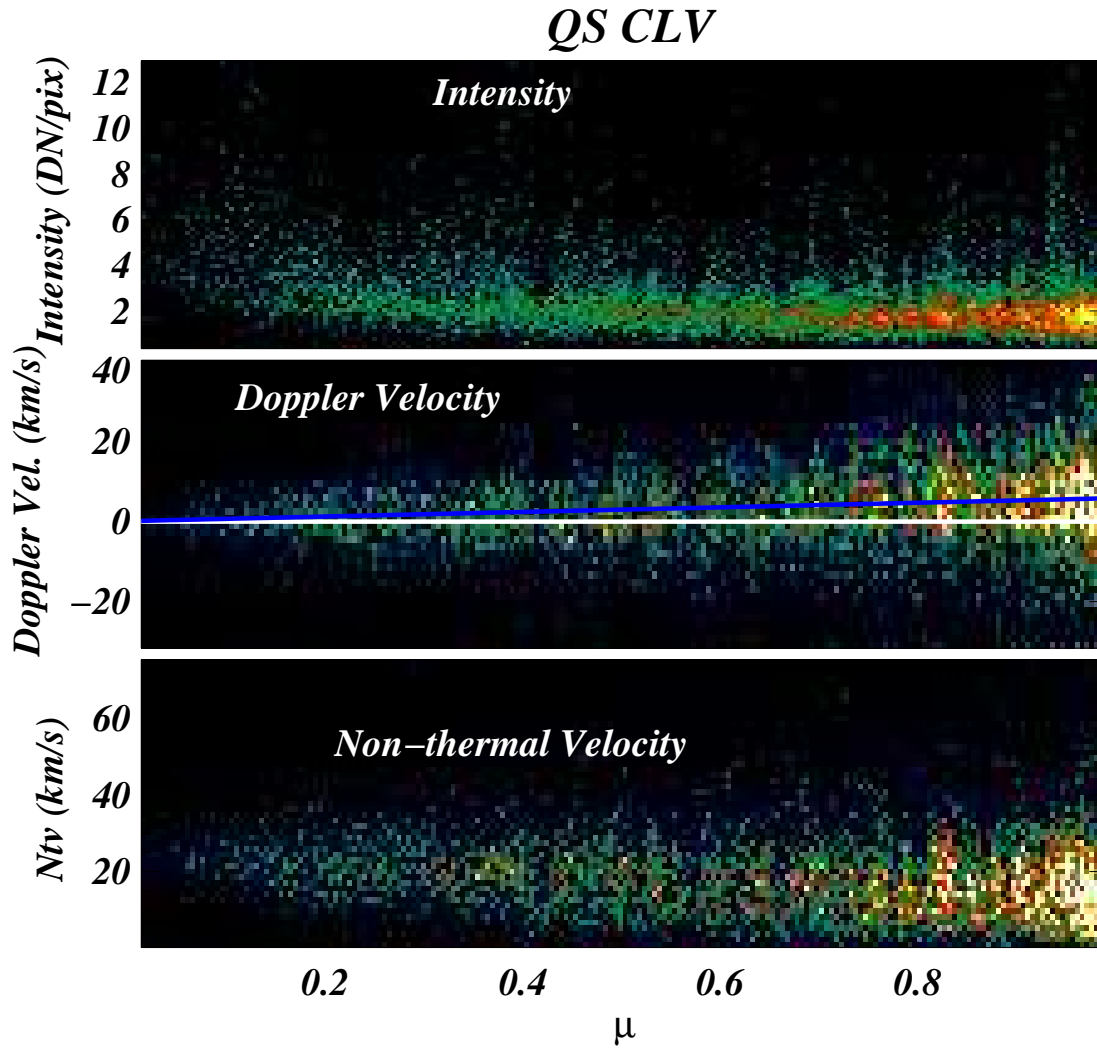


Figure 2. Two-dimensional histograms of spectral intensity (top panel), Doppler velocity (middle panel), and non-thermal velocity (bottom panel) plotted against μ for the QS region (the blue slanted patch in Figure 1). The blue line on the middle panel shows the fit to the Doppler velocity from Figure 4, and the white line denotes zero velocity.

- De Pontieu B., et al., 2014, *Sol. Phys.*, **289**, 2733
 Dere K. P., Bartoe J. D. F., Brueckner G. E., 1984, *ApJ*, **281**, 870
 Doschek G. A., Feldman U., Bohlin J. D., 1976, *ApJ*, **205**, L177
 Doyle J. G., Teriaca L., Banerjee D., 2000, *A&A*, **356**, 335
 Erdelyi R., Doyle J. G., Perez M. E., Wilhelm K., 1998, *A&A*, **337**, 287
 Feldman U., Doschek G. A., Patterson N. P., 1976, *ApJ*, **209**, 270
 Gunár S., Koza J., Schwartz P., Heinzel P., Liu W., 2021, *ApJS*, **255**, 16
 Hassler D. M., Rottman G. J., Orrall F. Q., 1991, *ApJ*, **372**, 710
 Hurlburt N., et al., 2012, *Sol. Phys.*, **275**, 67
 Kelly R. L., 1987, *Journal of Physical and Chemical Reference Data*, **17**
 Lemen J. R., et al., 2012, *Sol. Phys.*, **275**, 17
 Mariska J. T., 1992, *The Solar Transition Region*
 Pesnell W. D., Thompson B. J., Chamberlin P. C., 2012, *Sol. Phys.*, **275**, 3
 Peter H., 1999, *ApJ*, **516**, 490
 Peter H., Judge P. G., 1999, *ApJ*, **522**, 1148
 Rao Y. K., Del Zanna G., Mason H. E., 2022, *MNRAS*, **511**, 1383
 Rottman G. J., Hassler D. D., Jones M. D., Orrall F. Q., 1990, *ApJ*, **358**, 693
 Verbeeck C., Delouille V., Mampaey B., De Visscher R., 2014, *A&A*, **561**, A29
 Wilhelm K., et al., 1995, *Sol. Phys.*, **162**, 189

APPENDIX A: REST WAVELENGTH ESTIMATION: CENTRIOD VS μ

We have estimated the mean and standard deviation of the centroid at 100 μ values between 0.0 to 1.0 (disk center to limb). Please see section 3.1 for more details. The mean centroid versus μ is fitted with a straight line (see blue line in figure A.1). The fitted line is as follows: $y = 1402.7670 + 0.0243\mu$. Hence, the centroid at first μ value (i.e., at solar limb) is 1402.7670 Å, and it is considered as the rest wavelength of Si iv spectral line to calculate the Doppler velocity.

This paper has been typeset from a $\text{\TeX}/\text{\LaTeX}$ file prepared by the author.

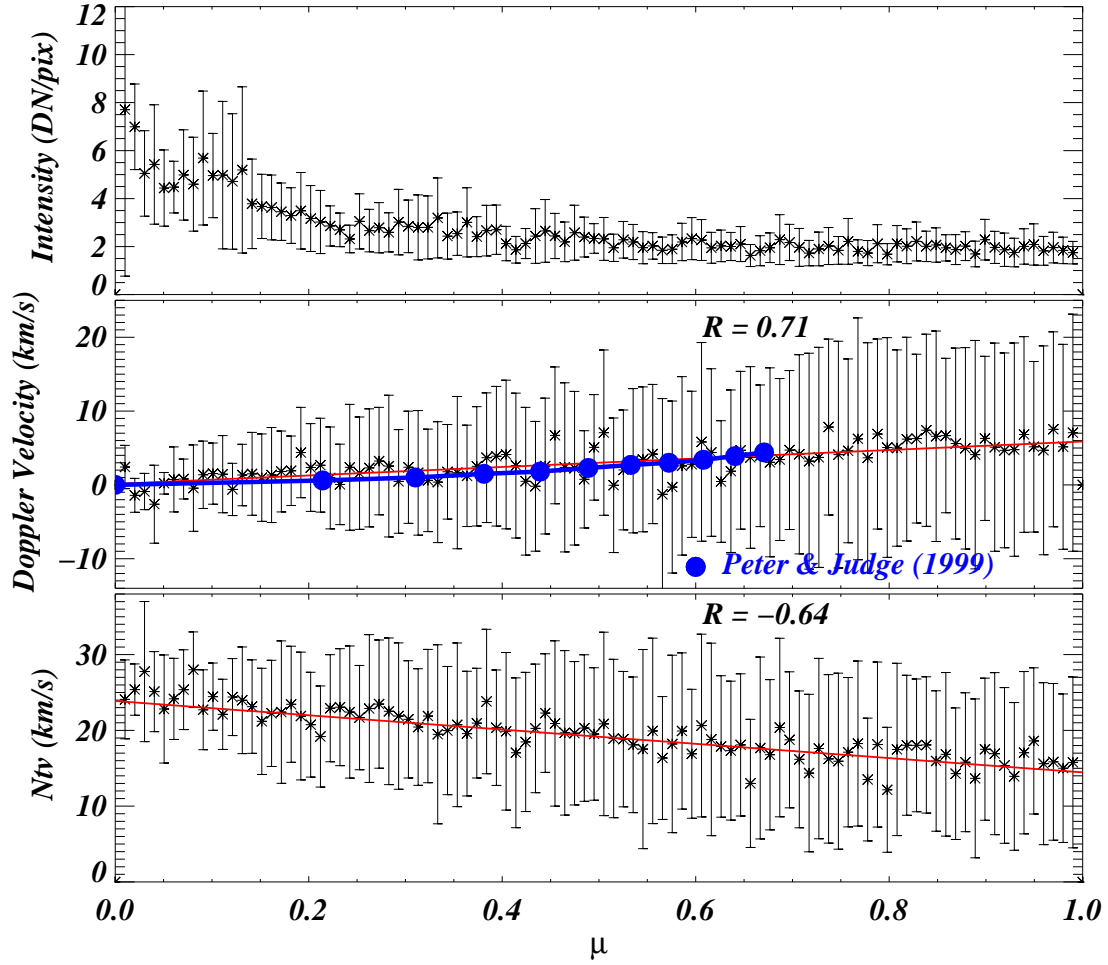


Figure 3. Plots of intensity (top), Doppler velocity (middle) and non-thermal velocity (bottom) averaged over 100 equally-spaced bins in μ . Linear fits to the Doppler velocity and non-thermal velocity are over-plotted in red, and the fit parameters are given in Table 1. The Pearson correlation coefficients, R , are displayed on the middle and bottom panels. The blue points on the middle panel are from Peter & Judge (1999).

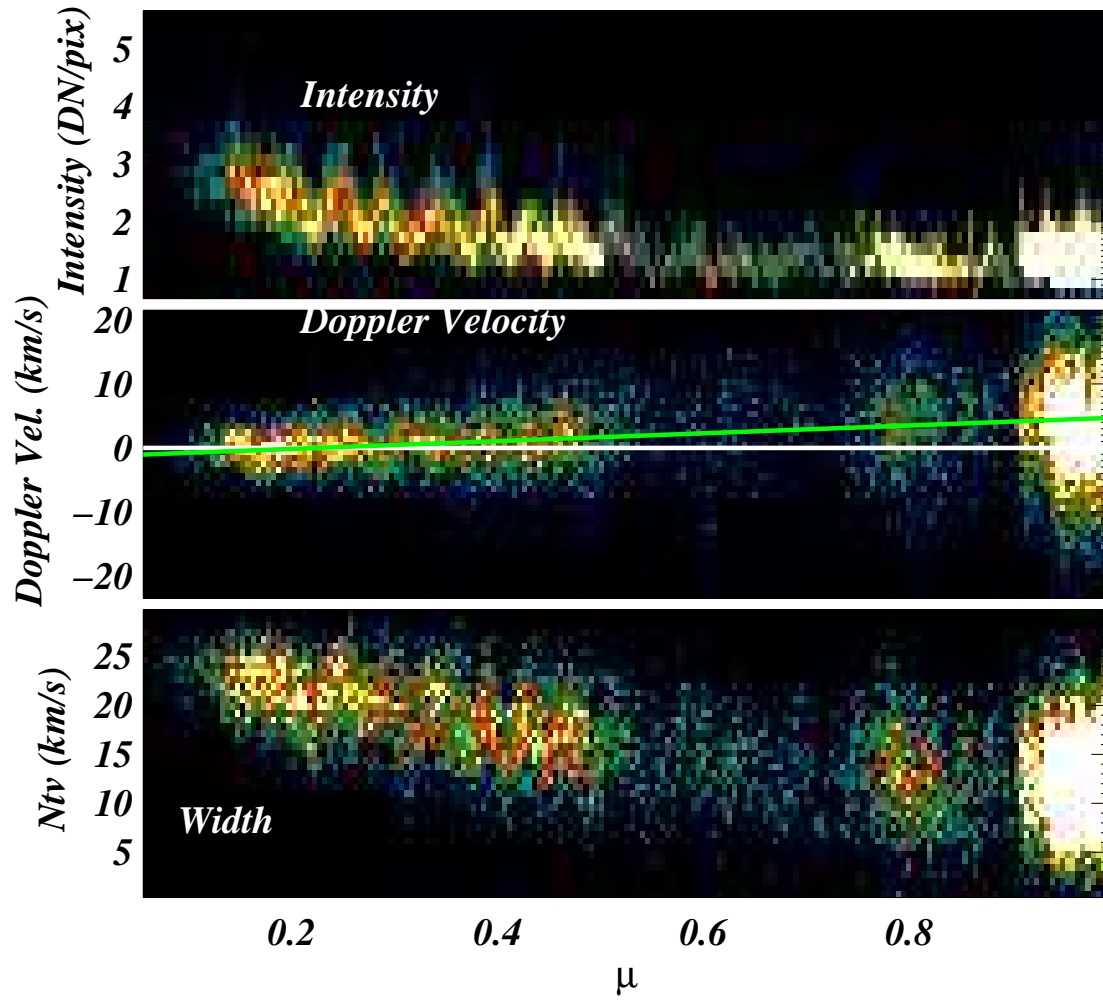


Figure 4. Two-dimensional histograms of spectral intensity (top panel), Doppler velocity (middle panel), and non-thermal velocity (bottom panel) plotted against μ for the CH region. The green line on the middle panel shows the fit to the Doppler velocity from Figure 3, and the white line denotes zero velocity.

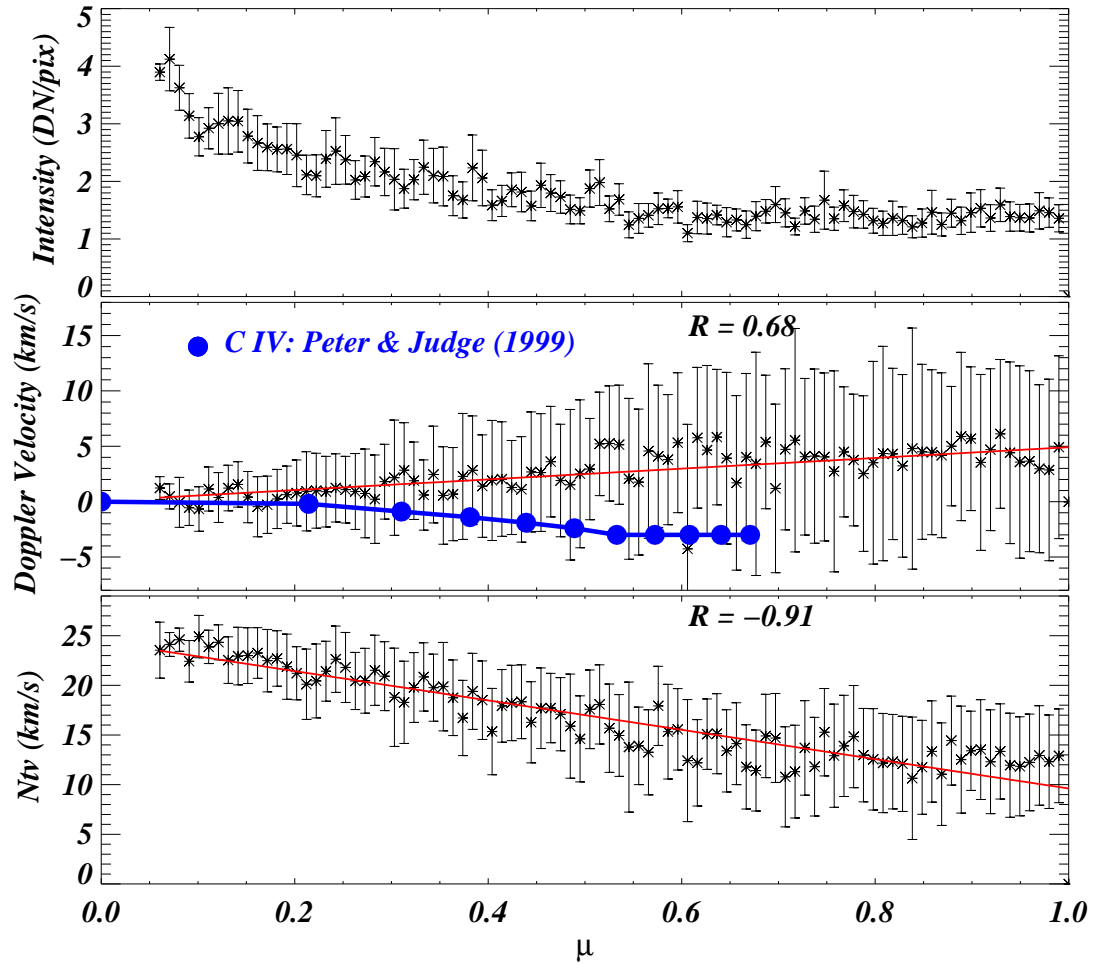


Figure 5. Same as Figure 3 but for the CH regions.

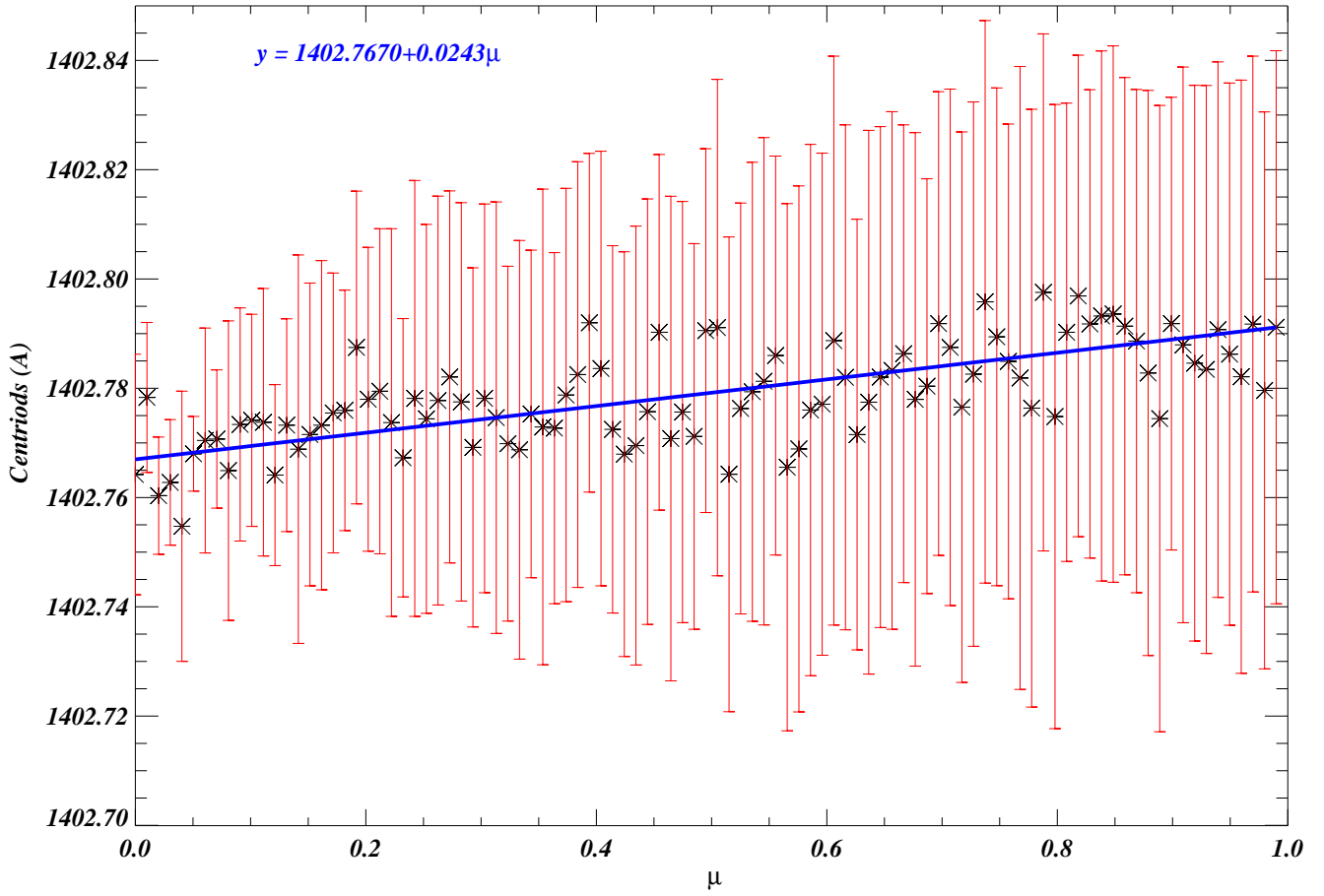


Figure A.1. The figure shows variations of centroid with μ values. The errors corresponding to each centroid are shown in red color. The blue line is the linear fit on the centroid, and the fitted line $y = 1042.7670 + 0.0243\mu$. Hence, the centroid at the limb is 1402.7670 Å (or 1402.77 Å) which is considered as the rest wavelength.